Predicting the Multipollutant Performance of Utility SCR Systems

Stephen Niksa*,† and April Freeman Sibley‡

Niksa Energy Associates LLC, 1745 Terrace Drive, Belmont, California 94002, and Southern Company Services, Inc., 600 N. 18th Street, Birmingham, Alabama 35203

This analysis relates catalyst material composition and bimodal pore size characteristics in a direct, quantitative way to the reactivities for simultaneous NO reduction, Hg^0 oxidation, and SO_3 production along utility selective catalytic reduction (SCR) reactors. SCR monoliths sustain two chemically distinct regions. In the inlet region, strong NH_3 adsorption minimizes the coverage of chlorinated and sulfated surface sites, so NO reduction inhibits Hg^0 and SO_2 oxidation. Once the NH_3 has been consumed, however, the chlorinated surface coverage surges by orders of magnitude, and the Hg^0 oxidation rate rapidly increases, even while the HCl concentration in the gas phase remains uniform. Ammonia inhibition also eliminates the benefit of the rapid film mass transfer at the SCR inlet from promoting Hg^0 oxidation. In many cases, the Hg^0 oxidation rate becomes limited by film transport soon after the Hg^0 begins to oxidize, so that none of the catalyst internal surface area is utilized. Shifting the pore size distribution toward macropores in a final catalyst stage appears to be an effective means for directly enhancing Hg^0 oxidation. The predictions were validated with pilot-scale data to demonstrate the crucial impact of NH_3 inhibition on SCR performance and with full-scale data for catalysts from a single vendor to show quantitative consistency across broad ranges of coal Cl content, gas hourly space velocity (GHSV), NH_3/NO ratio, and catalyst specifications.

Introduction

Selective catalytic reduction (SCR) technology has become the technology of choice worldwide to meet stringent NO_x emissions limits for coal-fired power plants. Along with NO reduction, SCR units also sustain Hg oxidation. The oxidation of elemental Hg (Hg^0) into oxidized Hg (Hg^{2+}) is important because only Hg^{2+} is water-soluble and therefore amenable to capture in flue gas desulfurization (FGD) scrubbing solutions. Extents of Hg^0 oxidation of 90% or more are routinely recorded in full-scale field tests,[1] provided that the flue gas contains abundant Cl or Br species and that the SCR system provides sufficient reactivity, favorable mass-transport rates, and ample residence time for the chemistry to proceed to near-completion. When these conditions are satisfied, SCR/electrostatic precipitator (ESP)/FGD combinations are also the technology of choice for Hg control because they require no special reagents or operating procedures to lower Hg emissions. Unfortunately, SCR catalysts inadvertently oxidize SO_2 into SO_3, and elevated SO_3 levels can significantly exacerbate plume opacity problems once the SO_3 condenses into fumes in the air preheater and beyond.

SCR is conducted on catalysts made by coprecipitation or impregnation of titania (TiO_2), vanadia (V_2O_5), tungsta (WO_3), and molybdina (MoO_3) into monoliths. Both honeycomb and plate monoliths are available with square, rectangular, circular, or triangular channels. Whereas the flue gas stream into the SCR inlet is turbulent, monoliths are sized to sustain independent laminar flows through individual channels. Temperature gradients across monoliths rarely exceed a few degrees, and operating pressures are near-atmospheric.

In such geometries, the reactant species must first traverse a developing laminar boundary layer along an inside channel wall and then penetrate the catalyst pore system to sustain the surface chemistry. One layer of analysis is needed to describe the concentration field as a function of axial position, z, and radial position within a channel, x. A second layer of analysis describes the competition between transport into the catalyst wall and reactant consumption through several surface reactions. A brute-force numerical rendering of all of the differential equations associated with a 2D flowfield and catalyst pore system is feasible, but such computations are notoriously unstable and computationally demanding, so they are unsuitable for extensive design studies and routine data interpretation.

Fortunately, SCR models have already advanced to the point where 2D formulations are unnecessary, and expedient substitutes give essentially the same answers in seconds on ordinary PCs, based on the following simplifications:

(1) Two-dimensional mass transport into the catalyst wall can be accurately rendered with correlations for square and circular channels,[2−4] triangular channels,[5] and the more complex plate-type monoliths[6,7] with a nondimensional mass-transfer coefficient that varies with axial distance.

(2) Rate expressions for NO reduction[3] and SO_2 oxidation[4] have already been reduced to their simplest possible forms for utility gas cleaning systems. Although the kinetic foundations for rates of Hg^0 oxidation are not nearly as extensive, our Hg^0 oxidation mechanism[8] depicts the essential parametric dependences, including interference due to competitive adsorption of NH_3 and HCl.

(3) The common characteristics among the reactivities for NO reduction, SO_2 oxidation, and Hg^0 oxidation are that (a) NH_3 strongly inhibits all three processes and (b) all rates are directly proportional to the concentrations of the primary reactant. Otherwise, SO_2 oxidation is weakly promoted by NO and O_2 and weakly inhibited by moisture, whereas Hg^0 oxidizes in proportion to the surface coverage of a chloride species supplied by HCl adsorption, which has a strong affinity for V_2O_5.[9] This coverage varies along the catalyst length even while the concentration of HCl vapor remains uniform because HCl is not consumed in any chemical process other than Hg^0

* To whom correspondence should be addressed. E-mail: neasteve@pacbell.net.
† Niksa Energy Associates LLC.
‡ Southern Company Services, Inc.

10.1021/ie9020599
Published on Web 06/17/2010

oxidation, and the Hg^0 concentration is orders of magnitude smaller than all other reactant concentrations.

(4) SO_2 oxidation is slow enough that all mass-transport restrictions are deemed to be negligible.[4]

(5) Concentration profiles of the species participating in NO reduction and Hg^0 oxidation can be based on closed-form analytical solutions for the validated rate expressions, and the numerical analysis does not need to resolve anything into the catalyst wall.[2,4,7,10,11]

The above simplifications have already been shown to provide results for simultaneous NO reduction and SO_2 oxidation that match more comprehensive numerical analyses.[2,3,12] An analysis of simultaneous NO reduction and Hg^0 oxidation in terms of a lumped overall reactivity for the combined influences of pore transport and surface conversion interpreted extents of Hg^0 oxidation by Cl species in laboratory-, pilot-, and full-scale SCR units for the complete domain of utility gas cleaning conditions[8] and was recently expanded for oxidation by Br species.[13] The present work expands the original lumped analysis in two ways. First, this work incorporates simultaneous SO_2 oxidation, and second, it resolves internal pore diffusion of NO, NH_3, and Hg^0 across the catalyst wall thickness from the intrinsic reactivity of adsorbed species on the catalyst surface with a Thiele analysis, to directly relate catalyst morphology and composition to the multipollutant performance of the SCR reactor.

Mathematical Analysis

Our analysis incorporates the analytical solutions for the NO profiles through the catalyst wall developed by Tronconi and co-workers,[2,3] but we develop new analytical expressions for the concentration profiles of NH_3, HCl, and Hg^0 through the wall to more accurately depict the impact of NH_3 inhibition on the surface chemistry. The kinetics of NO reduction have been resolved into the following three stages: (1) The system exhibits Langmuir−Hinshelwood kinetics below 200 °C; (2) NO adsorption becomes impossible for hotter temperatures, so the behavior shifts to Eley−Rideal (ER) kinetics; and (3) above 400 °C, adsorbed lattice oxygen oxidizes adsorbed NH_3 to produce N_2O, in parallel with the NO reduction sequence. As a result of the two later stages, r_{NO} passes through a maximum around 400 °C due to NH_3 oxidation. We therefore adopt ER kinetics for applications under utility gas cleaning conditions, where operating temperatures are always between 300 and 400 °C, according to the expression

$$r_{NO} = k_{NO}\frac{K'_{NH_3}C^S_{NH_3}}{1 + K'_{NH_3}C^S_{NH_3}}C^S_{NO} \quad \text{where} \quad K'_{NH_3} = \frac{K_{NH_3}}{1 + K_{HCl}C^S_{HCl}} \tag{1}$$

where k_{NO}, K_{NH_3}, and K_{HCl} have the Arrhenius form. All of the parameters associated with NO reduction must be regarded as adjustable, except that the true activation energy for NO reduction should be between 5 and 10 kcal/mol.

The stream concentrations of NO and NH_3 are described by

$$\frac{d\Phi_{NO,G}}{dZ^*} = -4Sh_{NO}(\Phi_{NO,G} - \Phi_{NO,S}) \quad \text{where} \quad \Phi_{NO,G}(0) = 1 \tag{2a}$$

$$\Phi_{NH_3,G} = \Phi_{NO,G} + \alpha - 1 \tag{2b}$$

$$Sh_{NO}(\Phi_{NO,G} - \Phi_{NO,S}) = \phi_{NO}\left\{\Phi_{NO,S}{}^2 - Y_0{}^2 + 2(S_1 - S_2) \times \left[\Phi_{NO,S} - Y_0 - S_2 \ln\left(\frac{\Phi_{NO,S} + S_2}{Y_0 + S_2}\right)\right]\right\}^{1/2} \tag{3}$$

where Φ_i denotes the concentration of NO or NH_3 normalized by the NO level at the SCR inlet; subscripts G and S denote free-stream and interfacial conditions on the channel wall, respectively; Z^* is a Graetz coordinate, given by $z/D_H Re \cdot Sc$; α is the molar NH_3/NO ratio; the effective diffusivities are evaluated from the random pore model;[14] and Sh_{NO} is a Sherwood number as a function of Z^*[2,3] given by

$$Sh_i = \frac{k_m D_H}{D_i} = Nu_{\infty,T} + 8.827(1000Z^*)^{-0.545}\exp(-48.2Z^*) \tag{4}$$

where $Nu_{\infty,T}$ depends on channel shape. In eq 3, the variables on the right-hand side are defined as follows

$$S_1 = \frac{D_{NH_3,EFF}}{D_{NO,EFF}}\Phi_{NH_3}(s) - \Phi_{NO}(s) \tag{5a}$$

$$S_2 = S_1 + \frac{D_{NH_3,EFF}}{K'_{NH_3}D_{NO,EFF}} \tag{5b}$$

and

$$Y_0 = \begin{cases} 0 & \text{if} \quad S_1 \geq 0 \\ -S_1 & \text{if} \quad S_1 < 0 \end{cases} \tag{5c}$$

where s is the wall half-thickness.

To gauge the mediation of the surface kinetics for NO reduction, an effectiveness factor is evaluated from the concentration profiles as

$$\eta_{NO} = \left[\frac{\phi_{NO}D_{NO}}{sD_H r_{NO}(C_{i,S})/C_{NO,S}}\right]\left\{\Phi_{NO,S}{}^2 - Y_0{}^2 + 2(S_1 - S_2) \times \left[\Phi_{NO,S} - Y_0 - S_2 \ln\left(\frac{\Phi_{NO,S} + S_2}{Y_0 + S_2}\right)\right]\right\}^{1/2} \tag{6}$$

The oxidation of SO_2 expresses a deeper interaction among more species than are involved in NO reduction, and several very complicated rate expressions have been reported. We confine our attention to one that has been shown to be capable of extrapolating from idealized test conditions to SCR performance with simultaneous NO reduction on commercial catalysts,[4] which is

$$r_{SO_2} = k_{SO_2}\frac{(1 + bC_{NO})C^{n_{O_2}}_{O_2}C^{n_{H_2O}}_{H_2O}}{1 + {}^{SO_2}K'_{NH_3}C^S_{NH_3}}C^S_{SO_2} \tag{7}$$

The NH_3 equilibrium constant in this rate law is distinguished with a superscript SO_2 because only a portion of the adsorbed NH_3 appears to affect SO_2 oxidation, so this value will differ from the value in the denominator of eq 1. Both NO and O_2

are weak promoters, but H_2O is an inhibitor; values of $n_{O_2} = 0.064$ and $n_{H_2O} = -0.211$ have been implemented,[11] and b in the NO promotion term is 17.1 m^3/mol.[15]

Because r_{SO_2} is sufficiently low that all transport effects are negligible under commercial operating conditions, the SO_2 concentration is determined by a balance between advection and film transport into the pore system within the wall, which integrates to the following axial concentration profile

$$\Phi_{SO_2,G} = \exp\left(-\frac{Z^*}{Z_{SO_2}}\right) \tag{8}$$

with

$$Z_{SO_2} = \frac{1 + \left(\frac{Sh_{SO_2}}{\phi_{SO_2}^{\ 2}}\right)}{4Sh_{SO_2}\Delta_{SO_2}}$$

$$\phi_{SO_2}^{\ 2} = \frac{D_H\langle r_{SO_2}\rangle}{D_{SO_2}}\left(\frac{V_C}{S_C}\right)$$

$$\Delta_{SO_2} = \frac{D_{SO_2}}{D_{NO}}$$

where $\Phi_{SO_2,G}$ is the free-stream SO_2 concentration normalized by the inlet value; V_C/S_C is the volume-to-surface ratio of the catalyst wall; and $\langle r_{SO_2}\rangle$ is the mean SO_2 oxidation rate through the wall. Even though pore transport does not mediate the SO_2 oxidation rate, it does introduce gradients into the NH_3 wall profiles. Consequently, $\langle r_{SO_2}\rangle$ requires mean NH_3 and NO concentrations in the wall at each axial position, which are obtained from the following Thiele analysis

$$\frac{d^2\Phi_{NH_3}}{dX^2} = \phi_{NH_3}^{\ 2}\frac{\Phi_{NO}K'_{NH_3}\Phi_{NH_3}}{1 + K'_{NH_3}\Phi_{NH_3}} \quad \text{for all} \quad 0 < X < 1 \tag{9}$$

with

$$\phi_{NH_3}^{\ 2} = \frac{s^2k_{NO}}{D_{NH_3,EFF}} \tag{9a}$$

$$\frac{d\Phi_{NH_3}(0)}{dX} = 0 \tag{9b}$$

$$\Phi_{NH_3}(1) = \alpha \tag{9c}$$

$$\Phi_{NO} = \Phi_{NO,S} + \frac{D_{NH_3,EFF}}{D_{NO,EFF}}(\Phi_{NH_3} - \Phi_{NH_3,S}) = 1 + \Delta_{NH_3}(\Phi_{NH_3} - \alpha) \tag{10}$$

where X is normalized by the wall half-thickness and ΔNH_3 is the ratio of bulk diffusion coefficients, D_{NH_3}/D_{NO}. This system can be separated and integrated once and rearranged into

$$X = \frac{1}{\phi_{NH_3}}\int_{\Phi^0_{NH_3}}^{\Phi_{NH_3}}\left\{\frac{d\Phi_{NH_3}}{2\int_{\Phi^0_{NH_3}}^{\Phi_{NH_3}}\frac{[1 + \Delta_{NH_3}(\Phi_{NH_3} - \alpha)]K'_{NH_3}\Phi_{NH_3}}{1 + K'_{NH_3}\Phi_{NH_3}}d\Phi_{NH_3}}\right\}^{1/2} \tag{11}$$

The integral in the denominator can be evaluated analytically, which leaves only one integral to be evaluated numerically. The resulting profiles are then integrated again over the wall coordinate to evaluate the average NO and NH_3 concentrations, after which they are substituted into eq 7 to evaluate $\langle r_{SO_2}\rangle$.

The relatively detailed rate expressions for r_{NO} and r_{SO_2} reflect an abundance of kinetic studies that characterize all of the major parametric dependence in detail. The situation is not nearly as secure for Hg oxidation, for which rate expressions were developed to depict tests at pilot- and full-scale plants on commercial catalysts under commercial conditions, and detailed rate studies are just beginning to appear.[16] The main underlying premise is that SCR catalysts can accommodate both NH_3 and HCl adsorbates. Hence, a competitive adsorption process relates Hg^0 oxidation to NO reduction. Chlorinated sites sustain Hg^0 oxidation, whereas ammoniated sites sustain NO reduction. This competition is described with adsorption equilibrium constants for both species, albeit with no further resolution of the nature of the adsorption sites and their corresponding affinity to both basic and acidic species. Notwithstanding this ambiguity, the strong coupling between NO reduction and Hg^0 oxidation through competitive adsorption of NH_3 and HCl has been independently validated with an extensive series of laboratory tests.[16]

The rate of Hg^0 oxidation is far too low to perturb the HCl concentration across the SCR apparatus, because of the disparate inlet concentrations of HCl and Hg^0. This implies that the HCl concentration in the gas phase is uniform across the SCR reactor. However, the NH_3 concentration falls continuously with distance along the SCR reactor, and according to the NH_3 adsorption equilibrium, the surface coverage of adsorbed NH_3 also diminishes accordingly. Even though the HCl vapor concentration is uniform, the surface coverage of chlorinated sites grows because there are fewer adsorbed NH_3 species to compete for sites farther inside the channels.

Accordingly, an ER rate law is applied to Hg^0 oxidation, whereby the Hg^0 reactant is the vapor or very weakly adsorbed species, because the concentration of Hg^0 is far too low to sustain adsorption equilibrium; in other words, if Hg^0 participated in the oxidation as an adsorbed species, the time to reach a steady-state surface coverage would be unbelievably long. Accordingly, the rate of Hg^0 oxidation is given by

$$r_{Hg} = k_{Hg}\frac{K'_{HCl}}{1 + {}^{Hg}K'_{NH_3}C^S_{NH_3}}C^S_{Hg} \quad \text{where} \quad K'_{HCl} = \frac{K_{HCl}C^S_{HCl}}{1 + K_{HCl}C^S_{HCl}} \tag{12}$$

No values for any of the parameters in eq 12 have been reported, and as for SO_2 oxidation, we expect that the value of ${}^{Hg}K'_{NH_3}$ will differ from the values for the same parameter in eqs 1 and 7. Moreover, we found no measurements that determine any of the parameters in k_{Hg} or K_{HCl}, so these parameters must also be regarded as adjustable.

The Hg^0 concentration profile is determined from

$$\frac{d\Phi_{Hg,G}}{dZ^*} = -4Sh_{Hg}\frac{D_{Hg}}{D_{NO}}(\Phi_{Hg,G} - \Phi_{Hg,S}) \quad \text{where} \quad \Phi_{Hg,G}(0) = 1 \tag{13}$$

$$\frac{d^2\Phi_{Hg}}{dX^2} = \phi_{Hg}^{\ 2}\frac{K'_{HCl}\Phi_{Hg}}{1 + K'_{NH_3}\Phi_{NH_3}} \quad \text{for all} \quad 0 < X < 1 \tag{14}$$

with

$$\phi_{Hg}^{\ 2} = \frac{s^2k_{Hg}}{D_{Hg,EFF}} \tag{14a}$$

$$\frac{d\Phi_{Hg}(0)}{dX} = 0 \quad (14b)$$

$$\frac{d\Phi_{Hg}(1)}{dX} = \Delta_{Hg} Sh_{Hg}[\Phi_{Hg,G} - \Phi_{Hg}(1)] \quad \text{where}$$

$$\Delta_{Hg} = \frac{sD_{Hg}}{D_H D_{Hg,EFF}} \quad (14c)$$

After applying the same transformation as was used to obtain eq 11, we find

$$X_{NH_3} + \int_{X_{NH_3}}^{1} \phi_{Hg}(X)\, dX = \int_{\Phi^0_{Hg}}^{\Phi_{Hg}(1)} \frac{d\Phi_{Hg}}{\left(2\int_{\Phi^0_{Hg}}^{\Phi_{Hg}} \Phi_{Hg}\, d\Phi_{Hg}\right)^{1/2}} = \int_{\Phi^0_{Hg}}^{\Phi_{Hg}(1)} \frac{d\Phi_{Hg}}{\left[\Phi_{Hg}{}^2 - (\Phi^0_{Hg})^2\right]^{1/2}} = \ln\left(\frac{1 + \sqrt{1 - \left(\frac{\Phi^0_{Hg}}{\Phi_{Hg}(1)}\right)^2}}{\frac{\Phi^0_{Hg}}{\Phi_{Hg}(1)}}\right) \quad (15)$$

where X_{NH_3} is the position within the wall where the NH_3 concentration might vanish, depending on the transport and reaction rates. The Hg^0 profile also determines the following effectiveness factor

$$\eta_{Hg} = \frac{\Phi_{Hg}(1)\sqrt{1 - \left(\frac{\Phi^0_{Hg}}{\Phi_{Hg}(1)}\right)^2}}{\phi_{Hg}} \quad (16)$$

These equations are solved with a Petzold−Gear routine for stiff coupled ordinary differential equations (ODEs) and algebraic equations. On a microprocessor operating at 1.5 GHz, each simulation takes less than 1 s.

Input Data Requirements

This analysis requires the following input data:

(1) the inlet gas concentrations of NO, HCl, and SO_2 (none of the other major gas components need to be specified provided that the O_2 and H_2O composition reflect typical coal-derived flue gases); (2) the total Hg concentration, in micrograms per dry standard cubic meter (μg/dscm), and the fraction of oxidized Hg at the SCR inlet; (3) the molar NH_3/NO ratio, which equals the measured NO conversion efficiency in practically all commercial DeNO_x systems; (4) the SCR temperature or an axial temperature profile if the temperature gradient exceeds 30 °C; (5) the gas hourly space velocity (GHSV), which is a nominal number of reactor volumes processed per hour, based on the flow rate at the SCR inlet evaluated at 0 °C; (6) the pitch and channel shape for both honeycomb and plate catalysts (although the wall thickness can be estimated from reported characterization data, it should also be specified as a measured value); (7) the mean sizes in the bimodal catalyst pore size distribution, along with the associated void fractions in each size class; and (9) the catalyst manufacturer, to provide a basis for clarifying geometric specifications and for estimating rate parameters.

Monolith pitch is the characteristic dimension of the unit cell. It is easiest to evaluate as the sum of the wall thickness and the opening size. Based on reported wall thicknesses from manufacturer's Web sites, wall thicknesses are typically 10% of the pitch. Such values typically yield flow voidages approaching 80% and geometric surface areas ranging from 300 to 900 m^2/m^3. Honeycomb monoliths can have square, circular, or triangular channels. The hydraulic diameter, D_H, that appears in the governing equations is evaluated as 4 × (flow area/wetted perimeter), where that flow area and perimeter are based on the open channel size (given by the difference between the pitch and the wall thickness).

Validation Database

All validation data in this article were obtained with Cormetech catalysts, to minimize uncharacterized variations in the intrinsic reactivities. The pilot-scale data sets from the Mercury Research Center (MRC) characterized regulated variations in flue-gas Cl level, flue-gas flow rate, and NH_3/NO ratio with sampling at intermediate and outlet positions, as explained elsewhere in more detail.[17] The MRC operates as a 5 MW slipstream facility, utilizing flue gas extracted from upstream and downstream of the economizer in the gas cleaning system at Plant Crist. It contains an SCR reactor, a Ljungstrom-type air preheater, an ESP, a pulse-jet fabric filter, and a wet FGD apparatus. The SCR reactor operates with diluted anhydrous NH_3 injected through a grid upstream of turning vanes and a flow straightener at the reactor inlet. The SCR catalyst is a honeycomb monolith with square channels of 7.1-mm pitch. It was installed in three layers at a total volume over 4 m^3. For the design flow rate, the gas hourly space velocity is 2913 h^{-1} at 0 °C. During the entire SCR test campaign, Plant Crist was operated on a Columbian high-volatile (hv) bituminous coal with only 0.02 wt % Cl, which is estimated to give an inherent flue-gas Cl concentration of only 14 ppmv. Speciated Hg concentrations were acquired at the SCR inlet, an intermediate position, and the SCR outlet with semicontinuous emissions monitors (SCEMs) at the extreme sampling positions and with a Tekran analyzer at the intermediate position. Flue-gas flow rates, temperatures, and inlet NO and O_2 levels were also recorded. Separate test series characterized the baseline design operation; variations in injected HCl ranged from 0 to 150 ppm; in flue-gas flow rate, from 75% to 125% of the design flow rate; and in the injected NH_3/NO ratio, from 0 to 0.95.

We also validate the predictions with a database on Hg transformations across full-scale SCR reactors that included most of the required characterization data.[1,18−20] The test teams monitored Hg vapor speciation at the SCR inlets and outlets at seven stations rated from 650 to 1300 MW. Four different SCR catalyst manufacturers were represented, although only the four sites with Cormetech honeycomb monoliths are included here. All coals were hv bituminous from mines in either the midwestern or eastern United States, except for the subbituminous burned at S1 and the subbituminous/bituminous blend burned at S8. However, the subbituminous at S1 generated an unusually high proportion of Hg^{2+}, because of the high unburned carbon (UBC) level from this cyclone furnace. The Cl-contents of the hv bituminous coals were typical, except for the relatively low values in the coals from S4.

The test sites were characterized in terms of the furnace rating; firing configuration; in-furnace control technologies for NO_x, SO_x, and particulates; SCR catalyst vendor and type; space velocity, and age. The most important specifications are collected in Table 1. Whereas NO_x conversion efficiencies were

Table 1. Operating Conditions of Full-Scale Cormetech Honeycomb SCR Reactors

site	T (°C)	GHSV (h^{-1})	HCl (ppm)	NO (ppm)	NH_3/NO	pitch (mm)
S1	383	1800	4	900	0.90	8.2
S4-1	363	2275	24	730	0.91	8.2
S4-2	363	2275	15	600	0.91	8.2
S6	−	3800	79	330	0.85	7.1
S8	336	3100	49	−	−	7.1

not reported, the inlet and outlet NO levels and NH_3 slip were. As expected, the NH_3 slip levels were usually well below 1 ppm, so NO_x conversion efficiencies were assigned from the NO concentrations across the SCR reactor, and the NH_3/NO ratios were set to the same values. Site S4 was monitored again after approximately one year. In the table, the label followed by "-2" denotes the second round of testing at the same site. Collectively, these sites cover essentially the entire range of SCR operating conditions in coal-fired power plants, except for catalyst manufacturer and whether the monolith is in plate or honeycomb configuration.

Simulation Results

For each test series, each test was simulated by entering the reported operating conditions into the computerized implementation of the analysis. Because no detailed porosity distribution data were reported, the default values for the MRC data set ($\varepsilon_\mu = 0.43$ for 70 Å; $\varepsilon_M = 0.015$ for 3000 Å) gave a highly microporous pore system. For the full-scale SCR reactors, the specifications were $\varepsilon_\mu = 0.43$ for 600 Å and $\varepsilon_M = 0.07$ for 5000 Å. Although these default values are plausible, they were standardized simply for lack of detailed information.

In the calculation sequence, an early calculation loop used the coal properties to assign a complete flue-gas composition by varying the air flow rate to match the estimated flue-gas O_2 concentration to a reported value. The governing equations were then solved to determine extents of NO reduction, SO_2 oxidation, and Hg^0 oxidation along the subject monolith. The predicted extents of $DeNO_x$ essentially equaled the specified NH_3/NO ratio for each test, even for the case with the greatest flue-gas flow rate, so these data are not shown here. Also, even though SO_3 levels were not monitored in any of the tests, the predicted values for the full-scale tests are shown but only to demonstrate their reasonable magnitudes, without any formal validation.

At this point in the model development, rate parameters must be adjusted to tune the predictions to the measured values for each catalyst manufacturer. To minimize these adjustments, one set was assigned from the MRC data sets, and another set was assigned for all of the full-scale test data; that is, the same rate parameters were applied to all full-scale data sets, on the assumption that the pore size characteristics, the catalyst compositions, and thus the intrinsic reactivities were very similar. Then, without further parameter adjustments, simulations were run to cover the variations in HCl concentration, NH_3/NO ratio, temperature, monolith dimension, and so on.

We characterize the extents of Hg conversion across the SCR reactors by the extent of Hg^0 oxidation, ${}^{SCR}X_{Hg^0}$, which is defined as

$$ {}^{SCR}X_{Hg^0} = 100 \times \frac{{}^{IN}C_{Hg^0} - {}^{OUT}C_{Hg^0}}{{}^{IN}C_{Hg^0}} \qquad (17) $$

Because the total measured Hg vapor concentrations stayed the same across the SCR reactors, within measurement uncertainties, the definition of ${}^{SCR}X_{Hg^0}$ is not subject to variations in the total flue-gas flow rate. The main advantage of this parameter is that it eliminates inadvertent and often substantial variations in the proportion of Hg^{2+} at the SCR inlet from affecting the SCR performance index. With the MRC data, it was evaluated from the reported proportions of Hg^{2+} across the SCR by first estimating the proportion of Hg^0 as the difference with 100%, and then by applying the above definition, on the assumption that no particulate Hg forms at the elevated SCR operating temperatures.

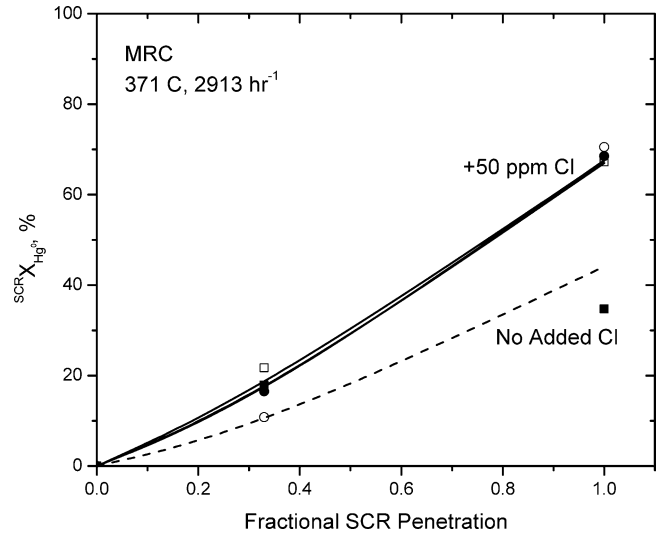

Figure 1. Evaluation of ${}^{SCR}X_{Hg^0}$ after the first layer and at the SCR exit for MRC design conditions with (□, ●, ○, and solid curves) and without (■ and dashed curve) 50 ppm injected Cl.

Evaluation with MRC Data Sets. The figures in this section cover the MRC test series on variations in flue-gas Cl level, flue-gas flow rate, and NH_3/NO ratio with sampling at intermediate and outlet positions. Each of these three variables was characterized in separate studies, and each of these three test series was repeated at a reference condition with 50 ppm injected Cl. The repeatability of these tests is seen in Figure 1, which shows the measured and simulated extents of Hg^0 oxidation at the intermediate and outlet positions. By definition, the values of ${}^{SCR}X_{Hg^0}$ are zero at the SCR inlet. With 50 ppm added Cl, the measured values grew to 18% after the first catalyst layer and then reached 70% at the SCR outlet. The simulations agree with these values throughout the SCR reactor within the measurement uncertainties and show that the first catalyst layer oxidized relatively little Hg^0 because of inhibition by the high NH_3 concentration. Note that the measured outlet values with Cl addition varied only from 67% to 71%, whereas the intermediate values varied from 11% to 22%. The measurement uncertainties at the intermediate sampling position were considerably greater than those at the outlet position because of the different Hg monitors and sampling protocol. The three simulations with Cl addition are not identical because of small variations in the flue-gas O_2 and NO levels in the tests. Without Cl injection, the measured value of ${}^{SCR}X_{Hg^0}$ is the same at the intermediate position, but it reaches only 35% at the SCR exit. The simulated values are lower throughout the SCR reactor without Cl injection but grow to 44% at the SCR exit. They clearly exhibit the correct tendency for smaller extents of Hg^0 oxidation for lower Cl levels in the flue gas.

The Cl dependence is characterized over a much broader range in Figure 2. As the level of injected Cl in the flue gas was increased from 0 to 150 ppm, the measured values of

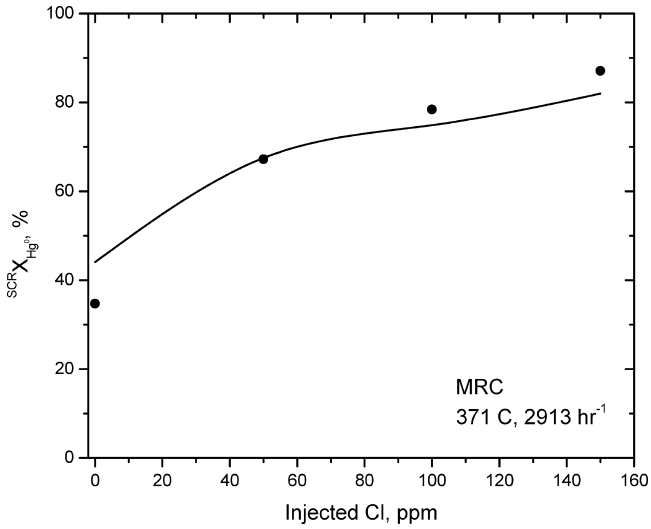

Figure 2. Evaluation of $^{SCR}X_{Hg^0}$ for MRC design conditions with up to 150 ppm injected Cl.

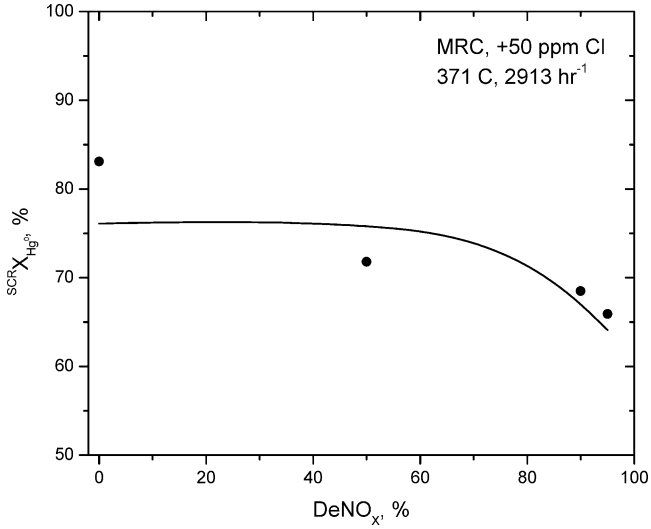

Figure 3. Evaluation of $^{SCR}X_{Hg^0}$ for MRC design conditions with 50 ppm injected Cl for a range of NH_3/NO ratios.

$^{SCR}X_{Hg^0}$ grew from 34% to 87%. The simulated values grew from 44% to 82% across this range. We attribute the discrepancy in the simulated value without Cl injection to uncertainties in the reported coal Cl level, because variations in coal Cl are inevitable during the course of any extended test campaign like this one. The simulated value would agree with the measured value without Cl injection if the coal Cl level were halved, which would not be an inordinate variation for low coal Cl values. The simulated values are within the measurement uncertainties with 50 and 100 ppm added Cl, but they are low by 5% with 150 ppm. Nevertheless, the simulation results accurately depict the strong Cl dependence for injection levels less than 50 ppm and the much weaker dependence for greater injection levels.

The inhibition of Hg^0 oxidation by NH_3 adsorption is clearly evident in the lower measured values of $^{SCR}X_{Hg^0}$ for progressively greater extents of $DeNO_x$ in Figure 3. We equate $DeNO_x$ and the NH_3/NO ratio on a percentage basis because the differences between the NH_3/NO set points in the tests and the measured extents of $DeNO_x$ showed only small random fluctuations. The greatest ratio of 0.95 gave 93.2% $DeNO_x$, consistent with expectations for such a high NH_3/NO ratio. The differences were smaller in the three replicate tests with a ratio of 0.9, as

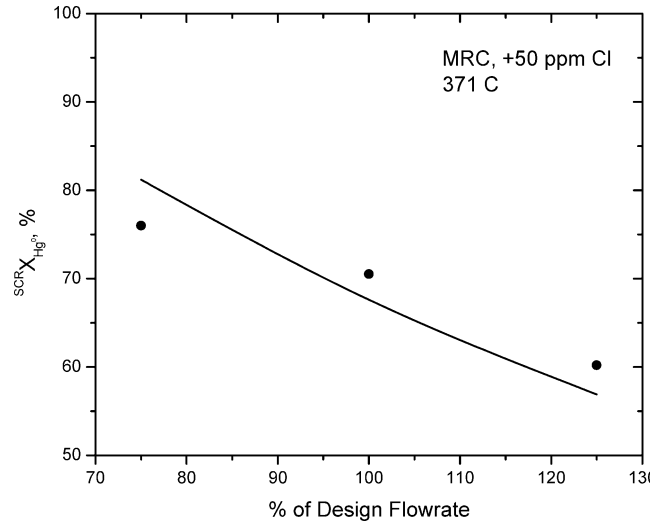

Figure 4. Evaluation of $^{SCR}X_{Hg^0}$ for MRC design conditions with 50 ppm injected Cl for a range of flue-gas flow rates.

expected. Apparently, this SCR reactor is slightly oversized for a ratio of 0.9 but might be insufficient for ratios that approach unity. As seen in Figure 3, the values of $^{SCR}X_{Hg^0}$ diminish for progressively greater NH_3/NO ratios, especially for ratios approaching unity. The simulation results accurately depict this tendency. However, there are too few points for lower extents of $DeNO_x$ to quantitatively resolve the dependence. The two measured points for lower $DeNO_x$ appear to resolve an inflection point on the way toward an acute dependence for hardly any $DeNO_x$. The simulation results exhibit a dependence that saturates out with less than 70% $DeNO_x$. Bear in mind that the simulated behavior could have been substantially modified by choosing different reactivity parameters, so the particular form for this important dependence for low extents of $DeNO_x$ remains ambiguous, pending additional data. In commercial applications, modern SCR reactors are operated for at least 80% $DeNO_x$, where the simulations are already as accurate as they need to be.

Variations in the flue-gas flow rate are characterized in Figure 4. Values of $^{SCR}X_{Hg^0}$ diminish for progressively greater flow rates, simply because nominal residence times within an SCR are inversely proportional to flow rate. The simulated dependence is accurate across this entire range, although, again, it is difficult to resolve changes in the slope of this curve with only three measurements.

In a preliminary test series in the MRC, data were collected that specified values for $^{SCR}X_{Hg^0}$ for SCR temperatures of 353 and 405 °C. These values for $^{SCR}X_{Hg^0}$ are systematically greater than those in the later test series, presumably because of improved strategies to control the test conditions. However, the relative changes should be suitable for comparison with the simulated temperature dependence. With 50 ppm added Cl, the measured value of $^{SCR}X_{Hg^0}$ was about 1% greater for the lower SCR temperature. The simulated impact of temperature is roughly the same, with the value of $^{SCR}X_{Hg^0}$ at the lower temperature being greater by only 1.5%. Temperature is the least important SCR operating condition simply because utility SCR reactors are operated within a very narrow temperature range and the reaction mechanisms do not shift within this window.

Evaluation with Data from Full-Scale SCR Reactors. The evaluations with full-scale test data are subject to greater uncertainties because of the inherent variability of fuel properties and operating conditions in full-scale gas cleaning systems. All

Table 2. Evaluation of $^{SCR}X_{Hg^0}$ across Full-Scale SCR Reactors with Cormetech Catalysts

	$^{SCR}X_{Hg^0}$, %		X_{NO} (%)	X_{SO_2} (%)	NH_3	ΔSO_3
	measured	predicted	predicted	predicted	slip (ppm)	(ppm)
S1	16.7	28.0	89.0	2.49	0	6
S4-1	82.8	63.7	91.0	1.95	0.1	47
S4-2	50.0	53.2	91.0	1.95	0.1	36
S6	59.5	64.7	84.9	0.88	0.3	6
S8	86.9	73.6	85.0	0.99	0.1	6

four Cormetech monoliths were simulated with the same rate parameters. Only the fuel properties and SCR operating conditions were changed to match the values imposed during the tests. The evaluation results appear in Table 2. The results comprise the measured and predicted extents of Hg^0 oxidation; the predicted conversion efficiencies, X_{NO} and X_{SO_2}; the predicted NH_3 slip; and the predicted incremental increase in SO_3 across the SCR reactor. Based on exhaustive interpretations of nearly all published results from Hg field test program sponsored by the U.S. Department of Energy,[21] we expect experimental uncertainties of 10−15% of the total Hg inventory for data sets such as these. The agreement among the measured and simulated $^{SCR}X_{Hg^0}$ values is within this tolerance, except for the first series from S4, for which the discrepancy is 19.1%, The agreement is especially significant because none of the rate parameters were adjusted to depict the impact of substantial variations in coal quality and SCR operating conditions, because all tests had Cormetech monoliths. Moreover, the repeated tests at S4 one year after the initial series were predicted to give lower extents of Hg^0 oxidation for the same reactivity parameters, consistent with the data albeit in smaller magnitude. According to this analysis, inadvertent variations in the test conditions were responsible for the diminished performance, rather than any aspects of catalyst deactivation.

The predicted NH_3 slip was always well below 2 ppm, in accord with the regulatory standard. Only the data set from S8 had qualified data on SO_3 levels, which was a single value at the SCR outlet of 16 ppm. The analysis predicted an increase of 6 ppm across the SCR reactor, which would be consistent with the measured value if the level at the inlet were 10 ppm—a reasonable value for a coal with 1.35 daf (dry ash free) wt % sulfur, as was fired in this furnace. Although more such data evaluations are needed to draw definitive conclusions, the early indications are that the proposed Hg oxidation mechanism can represent how coal quality affects Hg oxidation, given test data on one coal to assign the rate parameters for the catalyst under consideration. The evaluation results in Table 2 are especially important in this application, because the HCl concentrations in this database range from 4 to 79 ppm, which is almost the entire range encountered in utility gas cleaning systems.

Multipollutant Performance. Based on the satisfactory performance of the analysis in interpreting the pilot- and full-scale data, simulations were run to illustrate the interaction among the mechanisms for conversion of the three pollutants along an SCR channel. The SCR operating conditions were specified from case S4-1 in the full-scale database, for which the conditions were 730 ppm NO and 24 ppm HCl in the flue gas, $NH_3/NO = 0.91$, $T = 362$ °C, and GHSV = 2275 h^{-1}. There was 1.6 ppb Hg in the flue gas, of which 12% was oxidized at the SCR inlet. There were 2417 ppm SO_2 and 15 ppm SO_3 at the SCR inlet. The monolith was a square Cormetech honeycomb with 8.2-mm pitch and an estimated wall thickness of 1.0 mm. The mean micropore size was estimated as 600 Å, and the microporosity was 0.43. The mean macropore size was 5000 Å, and the macroporosity was 0.07.

We characterize the extents of conversion across the SCR reactors with the conversion efficiencies, X_j, which are defined as

$$X_j = 100 \times \frac{^{IN}C_j - {}^{OUT}C_j}{^{IN}C_j} \tag{18}$$

where j denotes the primary reactant in NO reduction, SO_2 oxidation, or Hg^0 oxidation.

The baseline emissions control performance is apparent in Figure 5, which shows X_{NO}, X_{SO_2}, NH_3 slip, η_{NO}, X_{Hg}, and η_{Hg} as functions of axial distance along the monolith. The length coordinate has been scaled by the total length of the SCR reactor. The most important feature to note is that NO reduction occurs over the leading half of the SCR reactor, whereas the oxidation of both SO_2 and Hg is confined to the downstream half of the catalyst. This is a direct reflection of the NH_3 inhibition term in the conversion rates for both of these species and the fact that the NH_3 level diminishes continuously from the inlet until it vanishes after about 40% of the catalyst length. The NH_3 concentration must be reduced into the tens of parts-per-million range before both SO_2 and Hg^0 begin to oxidize at appreciable rates. This is favorable for SO_3 control, because NH_3 inhibition significantly reduces the effective residence time available for SO_2 oxidation and makes the SCR reactor perform like a much shorter unit in this respect. Conversely, NH_3 inhibition is a serious impediment to Hg^0 oxidation, again, because it reduces the effective residence time.

However, there is an even more significant adverse impact on Hg^0 oxidation. According to the Sherwood number correlation in eq 4, the film diffusion coefficient has a nominally infinite value at the SCR inlet and then dramatically diminishes over the first few percent of the catalyst length. This rapid film mass transfer enhances the NO reduction rate and thereby delivers the full potential of the optimization of monolith channel specifications on NO reduction efficiencies. In particular, the channels are sized to sustain developing laminar flow, for which the very rapid film mass transfer near the inlet ensures that most of the catalyst will be available to eliminate nearly all of the NH_3, as a means to control NH_3 slip. We also see from the low effectiveness factors for NO reduction in Figure 5 that NO reduction in SCR reactors is deliberately confined to a very thin layer of the catalyst wall (for which η_{NO} is on the order $10^{-2}-10^{-1}$) to ensure that the NO reduction rate remains higher than the pore diffusion rate. The slight reduction in η_{NO} with axial distance reflects the zeroth-order dependence on C_{NH_3} for elevated NH_3 levels and the transition toward a first-order dependence for values in the single-digit part-per-million range.

Unfortunately, NH_3 inhibition prevents the rapid mass transfer at the SCR inlet from promoting Hg^0 oxidation. In fact, the Hg^0 oxidation rate is so low at the SCR inlet that the effectiveness factor approaches unity (because the rate does not even compete favorably with pore diffusion). The continuous transition toward lower values of η_{Hg} reflects the acceleration of Hg^0 oxidation while NH_3 and its associated inhibition is eliminated, as well as the lower rate of film mass transfer for progressively greater distances into the monolith. In many cases, the Hg^0 oxidation rate becomes limited by film transport soon after the Hg^0 begins to oxidize. The longer it takes for Hg^0 oxidation to begin, the greater the chance that the rate will become limited by the film transport rate—and for film-transport-limited conditions, none of the catalyst internal surface area is utilized.

Impact of Catalyst Morphology. Perhaps the main limitation to evaluations with data is that the catalyst morphology had to

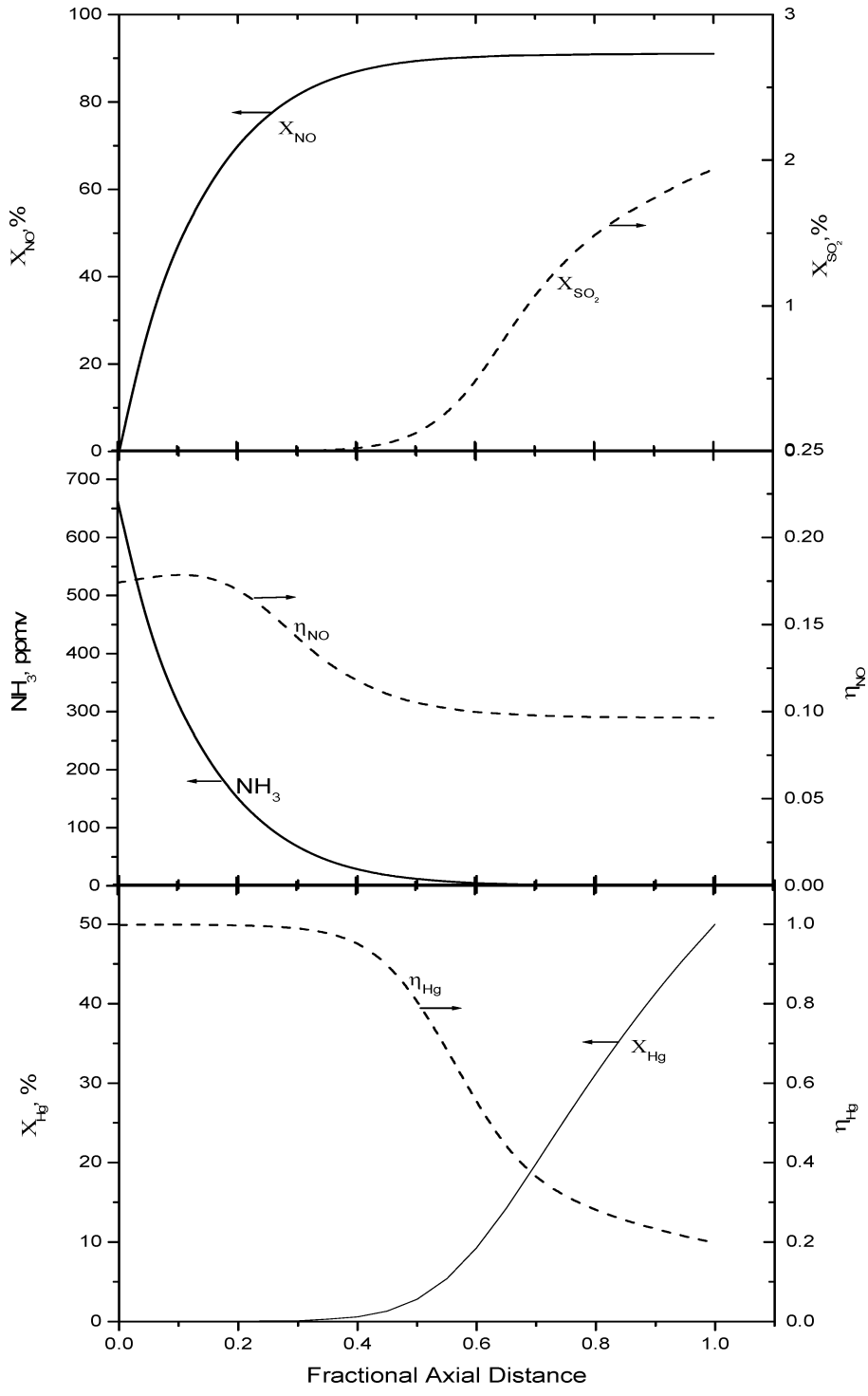

Figure 5. Predicted axial profiles of (top) X_{NO} (solid curve) and X_{SO_2} (dashed curve), (middle) NH_3 slip (solid curve) and η_{NO} (dashed curve), and (bottom) X_{Hg} (solid curve) and η_{Hg} (dashed curve) for an SCR reactor from a full-scale field test.

be assumed rather than based on direct determinations. To partially rectify this deficiency, the predicted impacts of variations in the most important morphological properties, the macroporosity and mean micropore size, appear in Figure 6. The micropore and macropore voidages were simultaneously adjusted to maintain the total porosity at 0.50, as required to maintain the monolith's structural integrity. The predicted extent of Hg^0 oxidation doubled from 39% to 77% as the macroporosity was increased from 0% to 32% (and the microporosity was correspondingly reduced from 50% to 18%). At first glance, this might be attributed to faster Hg transport through larger catalyst pore systems, which would increase the effectiveness factor for Hg^0 oxidation, η_{Hg}. In fact, the computed η_{Hg} values were smallest for the case with the most macropores, which is a direct reflection of the impact of the variations in pore volume on the consumption of NH_3 through NO reduction. For a greater percentage of macropores, η_{NO} increases and thereby accelerates NH_3 consumption. This weakens the inhibition of Hg^0 oxidation, which increases the oxidation rate, which, in turn, diminishes the η_{Hg} value.

To better resolve the impacts of a faster effective diffusivity for Hg^0 from diminished NH_3 inhibition, we repeated the study in Figure 6 for cases with an NH_3/NO ratio of only 1%. With no macropores, ${}^{SCR}X_{Hg^0}$ equaled 69%, but with 32% macroporos-

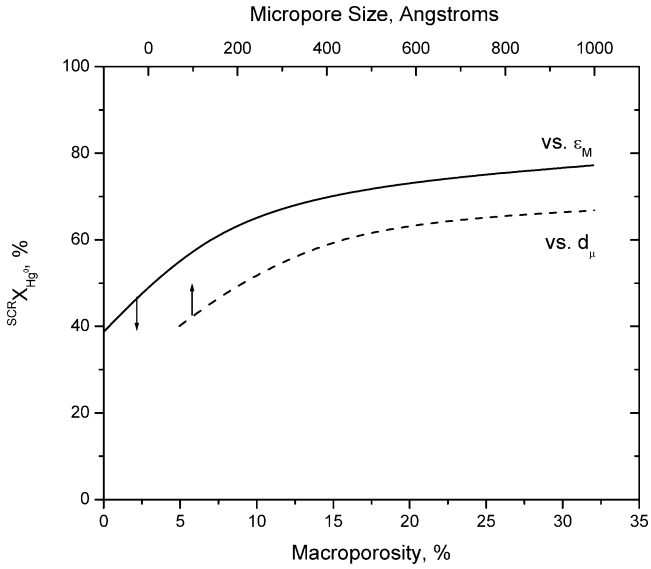

Figure 6. Predicted $^{SCR}X_{Hg^0}$ values for ranges of macroporosity and mean micropore size for case S4-1.

ity, $^{SCR}X_{Hg^0}$ grew to 91%. We can therefore attribute the bulk of the enhancement of $^{SCR}X_{Hg^0}$ in Figure 6 to the faster Hg diffusivity. In fact, the effective diffusivity for Hg increased from 9×10^{-7} to 1×10^{-4} m^2/s over this range of macroporosity. Shifting the pore size distribution toward macropores in a final catalyst stage would appear to be an effective means to directly enhance Hg^0 oxidation. According to our calculations, this strategy will not increase NH_3 slip, because it raises η_{NO}, nor will it increase X_{SO_2} by a significant amount, because transport effects are negligible in SO_2 oxidation. However, it does have the potential to significantly enhance $^{SCR}X_{Hg^0}$, all other SCR operating conditions being the same. It is also worth noting that most of the benefits in Figure 6 were realized in the increase in macroporosity from 0% to only about 8%, which makes this strategy potentially easier to implement. Increases in the micropore size also enhance Hg^0 oxidation, presumably because of the associated increases in the effective diffusivity of Hg. However, as seen in Figure 6, the impact is not as large as that for increases in macroporosity, and relatively greater adjustments are necessary. To gain most of the benefits, the micropore size needs to be increased to about 400 Å.

Discussion

This analysis quantitatively interprets the impacts of space velocity, NH_3/NO ratio, Cl level, and temperature on extents of Hg^0 oxidation along the SCR catalyst in the MRC, for the most part, within the measurement uncertainties. The interpretations for full-scale Cormetech SCR reactors are almost as accurate, although field-test data are necessarily subject to greater measurement uncertainties. The inhibition of Hg^0 oxidation by NH_3 adsorption in the MRC data sets corroborates the same effect that was previously characterized at laboratory,[16] pilot,[22] and full scale[1] (in tests with the NH_3 injectors turned off). Even though the quantitative form of this inhibition remains ambiguous for ratios below about 0.70, the proposed competitive adsorption between HCl and NH_3 accurately interprets the impact throughout the commercially important range of NH_3/NO ratios. Nevertheless, further characterization work with more penetrating analytical tools is needed to explain how acidic HCl and basic NH_3 exhibit strong adsorption affinities for common sites on the catalyst. It has been established that HCl strongly chlorinates V_2O_5 and that the promoters WO_3 and MoO_3 act as reservoirs for amine exchange onto V sites at some stage of the SCR of NO. At some point in this chain of interactions, sites form that can accommodate both adsorbed species, but the specific nature of these sites remains a mystery.

From the standpoint of commercial applications, the accuracy of the predictions is the most important consideration. This study has demonstrated that a single set of reactivity parameters and porosity characteristics can be specified from test data across a broad domain of SCR conditions to accurately depict the multipollutant performance of an SCR reactor. Once the parameters are specified in this way, users are in a position to apply the analysis to predict how coal switching will affect Hg emissions and SO_3 levels in existing installations. This information provides the best means to determine when additives are required to supplement the low Cl levels in some bituminous coals to maintain a specified level of Hg emissions control; how Hg emissions will vary across a furnace load curve; and how Hg emissions will be affected when the SCR is taken out of service, which has been demonstrated previously.[23]

The encouraging performance of the analysis for several full-scale SCR reactors from the same manufacturer suggests that families of reactivity parameters will ultimately be identified for different manufacturers and that fewer data will be needed over time to validate the predictions for different formulations from the same manufacturer. Toward this end, data taken on catalysts with known morphologies and chemical compositions would be especially valuable and could provide the means to accurately estimate the intrinsic reactivities of catalysts with different compositions with hardly any test data at all.

Conclusions

(1) The proposed ER mechanism for Hg^0 oxidation with competitive HCl and NH_3 adsorption quantitatively interprets the impacts of variations in Cl level, NH_3/NO, and gas flow rate.

(2) NH_3 adsorption simultaneously inhibits NO reduction, Hg^0 oxidation, and SO_2 oxidation. The adverse impact on Hg^0 and SO_2 oxidation is compounded by design features at the SCR inlet that sustain the highest mass-transfer rates under the maximum NH_3 concentration. Consequently, NO reduction is largely confined to the SCR inlet region, whereas Hg^0 and SO_2 primarily oxidize along the trailing region.

(3) The effectiveness factor for Hg^0 oxidation diminishes along the SCR reactor from near-unity at the inlet, where the rate is minimal. Under many commercial conditions, the oxidation rate becomes limited by film transport soon after Hg^0 begins to oxidize, and very little of the internal catalyst surface is utilized.

(4) Shifting the catalyst pore size distribution toward macropores significantly enhances Hg^0 oxidation, mostly because of the greater effective diffusivity for Hg^0 through larger pores. This strategy is not expected to increase NH_3 slip or enhance SO_2 oxidation.

(5) Increases in the mean micropore size also enhance Hg^0 oxidation, although the impact is not as large as with larger macropores and relatively greater adjustments are necessary.

Acknowledgment

This study was sponsored by Southern Company Services, Inc., and reflects their generous cooperation in providing detailed gas cleaning conditions for the MRC tests.

Nomenclature

A_X = flow cross section, m^2
b = proportionality constant in the NO dependence of r_{SO_2}
C_i = concentration of reactant i in the catalyst pore system, mol/m^3
$C_{i,G}$ = concentration of reactant i in the free stream, mol/m^3
$\langle C_i \rangle$ = average concentration of reactant i through the catalyst wall, mol/m^3
D_i = binary diffusivity of species i, m^2/s
$D_{i,EFF}$ = effective diffusion coefficient of species i through the catalyst pore system, m^2/s
D_H = hydraulic diameter = $4A_X/P$, m
$k_{m,i}$ = film mass-transfer coefficient of species i, m/s
k_j = rate constant for reaction j, 1/s
K_i = adsorption equilibrium constant for species i
${}^jK_i$ = adsorption equilibrium constant for species i for application with reaction j
$Nu_{\infty,T}$ = asymptotic value of the nondimensional mass-transfer coefficient for laminar channel flows
P = wetted perimeter, m
Re = Reynolds number
r_j = rate of surface reaction j, $mol/(m^3\ s)$
$\langle r_j \rangle$ = rate of surface reaction j evaluated at average concentrations, $mol/(m^3\ s)$
s = catalyst wall half-thickness, m
Sc_i = Schmidt number = $\mu/\rho D_i$
Sh_i = Sherwood number based on the transport properties of species i = $k_{m,i}D_H/D_i$
x = transverse distance into the catalyst pore system from the wall centerline, m
X = x/s
z = axial distance, m
Z^* = Graetz coordinate along a developing laminar boundary layer = $z/D_H Re \cdot Sc$
Z_{SO_2} = see eq 8

Greek Symbols

α = C_{NH_3}/C_{NO} at the inlet
Δ_i = D_i/D_{NO}
η_j = effectiveness factor for reaction j
Θ_i = fractional surface coverage of adsorbed species i
μ = gas viscosity
ρ = gas density
ϕ_j = Thiele modulus of reaction j
Φ_i = scaled concentration of species i through the catalyst pore system
$\Phi_{i,G}$ = scaled concentration of species i in the free stream
$\Phi_{i,S}$ = scaled concentration of species i at the interface with the channel wall

Subscripts

G = free-stream conditions
S = conditions at the interface between the free stream and the catalyst pore system

Superscripts

C_i^0 = inlet value of the free-stream concentration of species i
C_i^S = concentration of reactant i at the interface between the free stream and the catalyst, mol/m^3
Φ_i^0 = scaled concentration of species i at the centerline of the catalyst wall

Literature Cited

(1) Chu, P.; Laudal, D.; Brickett, L.; Lee, C. W. Power Plant Evaluation of the Effect of SCR Technology on Mercury. Presented at the U.S. EPA-DoE-EPRI Combined Power Plant Air Pollutant Control Symposium: The MEGA Symposium, Washington, DC, May 19−22, 2003.

(2) Tronconi, E.; Forzatti, P.; Gomez Martin, J. P.; Malloggi, S. Selective catalytic removal of NO_x: A mathematical model for design of catalyst and reactor. *Chem. Eng. Sci.* **1992**, *47* (9−11), 2401.

(3) Tronconi, E.; Forzatti, P. Adaquacy of lumped parameter models for SCR reactors with monolith structure. *AIChE J.* **1992**, *38* (2), 201.

(4) Svachula, J.; Alemany, L. J.; Ferlazzo, N.; Forzatti, P.; Tronconi, E. Oxidation of SO_2 to SO_3 over Honeycomb DeNoxing Catalysts. *Ind. Eng. Chem. Res.* **1993**, *32*, 826.

(5) Groppi, G.; Tronconi, E. Theoretical analysis of mass and heat transfer in monolith catalysts with triangular channels. *Chem. Eng. Sci.* **1997**, *52* (20), 3521.

(6) Giudici, R.; Tronconi, E. Laminar flow and forced convection heat transfer in plate-type monolith structures by a finite element solution. *Int. J. Heat Mass Transfer* **1996**, *39* (9), 1963.

(7) Beretta, A.; Orsenigo, C.; Forzatti, P.; Tronconi, E.; Forzatti, P.; Berti, F. Analysis of the performance of plate-type monolithic catalysts for SCR $DeNO_x$ applications. *Ind. Eng. Chem. Res.* **1998**, *37*, 2623.

(8) Niksa, S.; Fujiwara, N. A predictive mechanism for mercury oxidation on SCR catalysts under coal-derived flue gas. *J. AWMA* **2005**, *56*, 1866.

(9) Lisi, L.; Lasorella, G.; Malloggi, S.; Russo, G. Single and combined deactivating effect of alkali metals and HCl on commercial SCR catalysts. *Appl. Catal. B: Environ.* **2004**, *50*, 251.

(10) Tronconi, E.; Cavanna, A.; Forzatti, P. Unsteady Analysis of NO Reduction over Selective Catalytic Reduction−De-NO_x Monolith Catalysts. *Ind. Eng. Chem. Res.* **1998**, *37*, 2341.

(11) Tronconi, E.; Beretta, A. The role of inter- and intra-phase mass transfer in the SCR-$DeNO_x$ reaction over catalysts of different shapes. *Catal. Today* **1999**, *52*, 249.

(12) Beeckman, J. W.; Hegedus, L. L. Design of monolith catalysts for power plant NO_x emission control. *Ind. Eng. Chem. Res.* **1991**, *30*, 969.

(13) Niksa, S.; Naik, C. V.; Berry, M. S.; Monroe, L. Interpreting enhanced Hg oxidation with Br addition at Plant Miller. *Fuel Process. Technol.* **2009**, *90*, 1372.

(14) Aris, R. *The Mathematical Theory of Diffusion and Reaction in Permeable Catalysts*; Clarendon Press: Oxford, U.K., 1975; Vol. 1, The Theory of the Steady State.

(15) Tronconi, E.; Beretta, A.; Elmi, A. S.; Forzatti, P.; Malloggi, S.; Baldacci, A. A complete model of SCR monolith reactors for the analysis of interacting NO_x reduction and SO_2 oxidation reactions. *Chem. Eng. Sci.* **1994**, *439* (24A), 4277.

(16) Kamata, H.; Ueno, S.-I.; Naito, T.; Yukimura, A. Mercury oxidation over the $V_2O_5(WO_3)/TiO_2$ commercial SCR catalyst. *Ind. Eng. Chem. Res.* **2008**, *47*, 8136.

(17) Freeman Sibley, A.; Hinton, W. S.; Jienez, A.; Dene, C. Pilot-scale studies of mercury oxidation by SCR catalysts. Presented at the U.S. EPA-DoE-EPRI Combined Power Plant Air Pollutant Control Symposium: The MEGA Symposium, Baltimore, MD, Aug 25−28, 2008.

(18) Laudal, D. L.; Thompson, J. S.; Pavlish, J. H.; Brickett, L.; Chu, P.; Srivastava, R. K.; Lee, C. W.; Kilgroe, J. Evaluation of mercury speciation at power plants using SCR and SNCR control technologies. Presented at Air Quality III, Arlington, VA, Sep 9−12, 2002.

(19) Laudal, D. L.; Wocken, C. A.; Chu, P.; Brickett, L.; Lee, C. W. Evaluation of the effect of SCR on mercury speciation and emissions. Presented at the U.S. EPA-DoE-EPRI Combined Power Plant Air Pollutant Control Symposium: The MEGA Symposium and AWMA Specialty Conference on Mercury Emissions: Fate, Effects, and Control, Chicago, IL, Aug 21−23, 2001.

(20) Laudal, D. L.; Thompson, J. S.; Pavlish, J. H.; Brickett, L.; Chu, P.; Srivastava, R. K.; Lee, C. W.; Kilgroe, J. Mercury speciation at power plants using SCR and SNCR control technologies. *Environ. Manager* **2003**, (Feb), 16.

(21) Naik, C. V.; Krishnakumar, B.; Niksa, S. Predicting Hg emissions from utility gas cleaning systems. *Fuel* **2010**, *89*, 859.

(22) Machalek, T.; Ramavajjala, M.; Richardson, M.; Richardson, C. Pilot evaluation of flue gas mercury reactions across an SCR unit. Presented at the U.S. EPA-DoE-EPRI Combined Power Plant Air Pollutant Control Symposium: The MEGA Symposium, Washington, DC, May 19−22, 2003.

(23) Niksa, S.; Bour, D. P.; Burnett, T. A.; Handagama, N. B. Use predictive techniques to guide your mercury compliance strategy. *Power* **2007**, *151* (8), 60.

Received for review December 28, 2009
Revised manuscript received May 24, 2010
Accepted May 26, 2010

IE9020599